RNA polymerase II progression through H3K27me3-enriched gene bodies requires JMJD3 histone demethylase

Conchi Estarás[a,*], Raquel Fueyo[a], Naiara Akizu[a,†], Sergi Beltrán[b,‡], and Marian A. Martínez-Balbás[a]
[a]Department of Molecular Genomics, Instituto de Biología Molecular de Barcelona, Consejo Superior de Investigaciones Científicas, 08028 Barcelona, Spain; [b]Unitat de Bioinformàtica, Centres Científics i Tecnològics, Universitat de Barcelona, 08028 Barcelona, Spain

ABSTRACT **JMJD3 H3K27me3 demethylase plays an important role in the transcriptional response to different signaling pathways; however, the mechanism by which it facilitates transcription has been unclear. Here we show that JMJD3 regulates transcription of transforming growth factor β (TGFβ)–responsive genes by promoting RNA polymerase II (RNAPII) progression along the gene bodies. Using chromatin immunoprecipitation followed by sequencing experiments, we show that, upon TGFβ treatment, JMJD3 and elongating RNAPII colocalize extensively along the intragenic regions of TGFβ target genes. According to these data, genome-wide analysis shows that JMJD3-dependent TGFβ target genes are enriched in H3K27me3 before TGFβ signaling pathway activation. Further molecular analyses demonstrate that JMJD3 demethylates H3K27me3 along the gene bodies, paving the way for the RNAPII progression. Overall these findings uncover the mechanism by which JMJD3 facilitates transcriptional activation.**

Monitoring Editor
A. Gregory Matera
University of North Carolina

Received: Jul 27, 2012
Revised: Nov 26, 2012
Accepted: Nov 30, 2012

INTRODUCTION

Cellular identity and function are determined by a combination of signaling pathways that converge on chromatin to regulate the transcription of specific sets of genes. Thus chromatin is the final platform where cellular signals are integrated in order to control gene transcriptional programs. Chromatin accessibility is regulated by epigenetic mechanisms, particularly by covalent histone modifications. Among these, methylation of Lys-27 of histone H3 (H3K27me3) has been found to be a key regulator of cell homeostasis and embryonic development (Morey and Helin, 2010; Margueron and Reinberg, 2011). Enhancer of Zeste Homologues 1 and 2 (EZH1/2) are the enzymes responsible for the H3K27 methylation reaction (Cao *et al.*, 2002; Czermin *et al.*, 2002; Kuzmichev *et al.*, 2002). They are part of Polycomb repressive complex 2 (PRC2), which, together with the PRC1 complex, establishes the repressive state associated with H3K27me3 marks (Cao *et al.*, 2002; Lois *et al.*, 2010). Although H3K27me3 has been described as a stable histone mark, recent findings show that two new histone demethylase (HDM) enzymes, JMJD3 and UTX, can cause this modification to revert (Agger *et al.*, 2007; De Santa *et al.*, 2007; Lan *et al.*, 2007; Lee *et al.*, 2007). Both JMJD3 and UTX contain a Jumonji C (JmjC) domain responsible to the HDM catalytic activity (Agger *et al.*, 2007; De Santa *et al.*, 2007; Lan *et al.*, 2007; Lee *et al.*, 2007). These two genes play an essential role during development, as many key developmental promoters are often marked by H3K27me3 (Boyer *et al.*, 2006; Bracken *et al.*, 2006; Lee *et al.*, 2006; Pan *et al.*, 2007). In particular, they derepress *HOX* genes and a subset of neural and epidermal differentiation genes (Agger *et al.*, 2007; Jepsen *et al.*, 2007; Lan *et al.*, 2007; Lee *et al.*, 2007; Burgold *et al.*, 2008; Sen *et al.*, 2008). Moreover, it has recently been shown that JMJD3 cooperates with transforming growth factor β (TGFβ) and bone morphogenic protein signaling pathways to

This article was published online ahead of print in MBoC in Press (http://www.molbiolcell.org/cgi/doi/10.1091/mbc.E12-07-0561) on December 14, 2012.

Present addresses: *Regulatory Biology Laboratory, Salk Institute for Biological Studies, La Jolla, CA 92037-1099; †Department of Neurosciences and Pediatrics. University of California, San Diego, La Jolla, CA 92093-0665; ‡Center Nacional d'Anàlisi Genòmica, Parc Científic de Barcelona, 08028 Barcelona, Spain.

Address correspondence to: Marian A. Martínez-Balbás (mmbbmc@ibmb.csic.es).

Abbreviations used: ChIP-seq, chromatin immunoprecipitation followed by sequencing; FC, fold change; JDTA,TGFβ responsive genes that require JMJD3 to be activated; NSCs, neural stem cells; qPCR, quantitative PCR; RNAPII, RNA polymerase II; RNAPII-S2p, Ser-2 phosphorylated RNA polymerase II; TGFβ, transforming growth factor beta; TSS, transcription start site; TES, transcription end site.

control neuronal differentiation and cell fate specification in early neural development (Akizu *et al.*, 2010; Estarás *et al.*, 2012). These findings point to an important role of JMJD3 and UTX, and hence H3K27me3 demethylation, in transcriptional regulation of specific signaling pathways. However, the mechanism by which these enzymes facilitate transcription remains unclear. Of interest, genome-wide analyses recently showed that JMJD3 binds to promoters, but also to gene bodies, in neural stem cells (NSCs; Estarás *et al.*, 2012) and macrophages (De Santa *et al.*, 2009). In addition, it has been reported that UTX localizes at the intragenic regions of muscle-specific genes during myogenesis (Seenundun *et al.*, 2010). Moreover, recent data indicate that the H3K27me3 pattern moves from promoters to intragenic regions after cell differentiation (Hawkins *et al.*, 2010). When considered together, these data led us to hypothesize that H3K27me3 HDMs might play an important role at intragenic regions in transcriptional response to signaling pathway activation.

To address this hypothesis, we analyzed the contribution of gene-body–associated JMJD3 to TGFβ transcriptional response. Our data demonstrate that JMJD3 is required to promote transcription elongation by demethylating H3K27me3 at the transcribed regions of TGFβ-responsive genes.

RESULTS

Genome-wide H3K27me3 distribution in NSCs

Genome-wide analysis has shown that JMJD3 localizes on gene bodies in TGFβ-stimulated NSCs (Estarás *et al.*, 2012). However, we still do not know how the association of JMJD3 to intragenic regions contributes to TGFβ-mediated transcriptional response. To address this problem, we first analyzed the global H3K27me3 profile in NSCs by applying the chromatin immunoprecipitation followed by sequencing (ChIP-seq) technique (Figure 1A). First, we validated the H3K27me3 antibody by ChIP, followed by quantitative PCR (qPCR) of two well-known H3K27me3 targets and a negative control (Supplemental Figure S1A). Using the same conditions, we performed H3K27me3 ChIP assays; then libraries were generated and sequenced with an Illumina Genome Analyzer II. The total number of peaks detected after input normalization was 16,168.

We then examined the genomic distribution of the H3K27me3 peaks. Our results, in accordance with findings from other cell contexts (Hawkins *et al.*, 2010; Kim *et al.*, 2011), showed that the H3K27me3 mark is abundant within the intragenic regions (Figure 1B). More precisely, we identified 5009 H3K27me3 peaks along the gene bodies and 982 around the transcription start site (TSS; defined as ±1000 base pairs; Figure 1C). These results are in good agreement with previous data on specified cells (Hawkins *et al.*, 2010), showing that H3K27me3-binding sites are spread along the intragenic regions and decrease around the transcription end site (TES; Figure 1, D and E). A different distribution was described for embryonic stem cells (Barski *et al.*, 2007; Mikkelsen *et al.*, 2007), in which H3K27me3 is mainly localized around the TSS and promoters.

We previously showed that JMJD3 is essential to activate a set of TGFβ-induced genes in NSCs (Estarás *et al.*, 2012, and Figure 1F). To characterize the dynamics of H3K27 methylation, we analyzed the H3K27me3 levels in the set of TGFβ-responsive genes that require JMJD3 to be activated (fold change [FC] ≥ 1.5, $p \leq 0.05$; 61 genes), from now on abbreviated as JDTA genes (Figure 1F and Supplemental Table S1). Results in Figure 1G and Supplemental Figure S1B show that JDTA genes (Figure 1G, orange box) are enriched in H3K27me3 compared with the remaining genes in the array (20,636; Figure 1G, green box, and Supplemental Figure S1B).

JMJD3 associates with H3K27me3 gene bodies in TGFβ-stimulated NSCs

The results described in the preceding section suggest that H3K27 methylation/demethylation at the transcribing regions might play a pivotal role in TGFβ response. To test this hypothesis, we investigated the binding sites of JMJD3 in NSCs treated with TGFβ by ChIP-seq (Figure 2A). We first checked the efficiency of the JMJD3 antibody used in our experimental conditions (Supplemental Figure S2A). After sequencing of JMJD3-associated DNA fragments, we identified 61,610 peaks. In agreement with previous data (Estarás *et al.*, 2012) and consistent with what was identified in other cell contexts (De Santa *et al.*, 2009), JMJD3 peaks were distributed across the intergenic and intragenic regions (Figure 2B and Supplemental Figure S2B).

Next we compared the distribution of JMJD3 around TSS, TES, and gene bodies between JDTA genes and the remaining genes in the array. Results in Figure 2C show that the former exhibited higher levels of bound JMJD3 both in TSS and gene bodies. Remarkably, JMJD3 was distributed along the intragenic regions until the TES (Figure 2C).

We then examined whether JMJD3 binds H3K27me3 gene bodies upon TGFβ treatment. We observed that JMJD3 associates with the 90.9% of methylated genes (Figure 2D, orange box), suggesting that JMJD3 is recruited to these regions upon signal activation.

To further explore this idea, we tested whether TGFβ signal was required to recruit JMJD3 to gene bodies by ChIP followed by qPCR experiments. Results in Figure 2, E and F, show that, 3 h after TGFβ treatment, JMJD3 was recruited to the intragenic regions of the TGFβ-responsive gene neurogenin 2 (*Neurog2*; Estarás *et al.*, 2012). This recruitment was not observed for the gene *G6pd2* (Figure 2, E and F), a non–TGFβ-regulated gene used as a negative control. Of interest, Smad3 was not targeted to the intragenic region upon TGFβ treatment, suggesting that JMJD3 binding to the gene bodies is not led by Smad3 (Supplemental Figure S3A), in contrast to what was found for promoters (Estarás *et al.*, 2012). In addition, TGFβ signaling did not affect JMJD3 subcellular distribution (Supplemental Figure S3B). These findings reinforce the idea that the binding of JMJD3 to the intragenic regions facilitates transcription.

Because our data indicate that JDTA genes are enriched in H3K27me3 before TGFβ activation (Figure 2D), we tested whether the binding of JMJD3 to intragenic regions leads to H3K27me3 demethylation. To this end, we analyzed changes in H3K27me3 levels along the *Neurog2* gene body upon TGFβ activation. Results in Figure 2G indicate that H3K27me3 levels decreased 3 h after cytokine addition in the analyzed regions. To further characterize the contribution of JMJD3 to the observed demethylation, we analyzed the H3K27me3 levels in JMJD3 KD cells. As shown in Supplemental Figure S3C, no significant changes were detected in H3K27me3 levels in TGFβ-stimulated JMJD3 KD cells. These data demonstrate that the H3K27me3 demethylation observed in the intragenic regions of JDTA genes in control cells is dependent on JMJD3. This is supported by ChIP-seq data analysis, showing an overall lack of coincidence between nucleotides bound by H3K27me3 and JMJD3 (Supplemental Figure S3D). In summary, these results support the notion that JMJD3 association with gene bodies promotes H3K27me3 demethylation.

JMJD3 interacts with RNAPII-S2p

The results described here reveal an enrichment in JMJD3 along the gene body for JDTA genes. This suggests that JMJD3 might be involved in RNAPII elongation. To explore this hypothesis, we investigated the association of JMJD3 with elongating RNAPII. Using

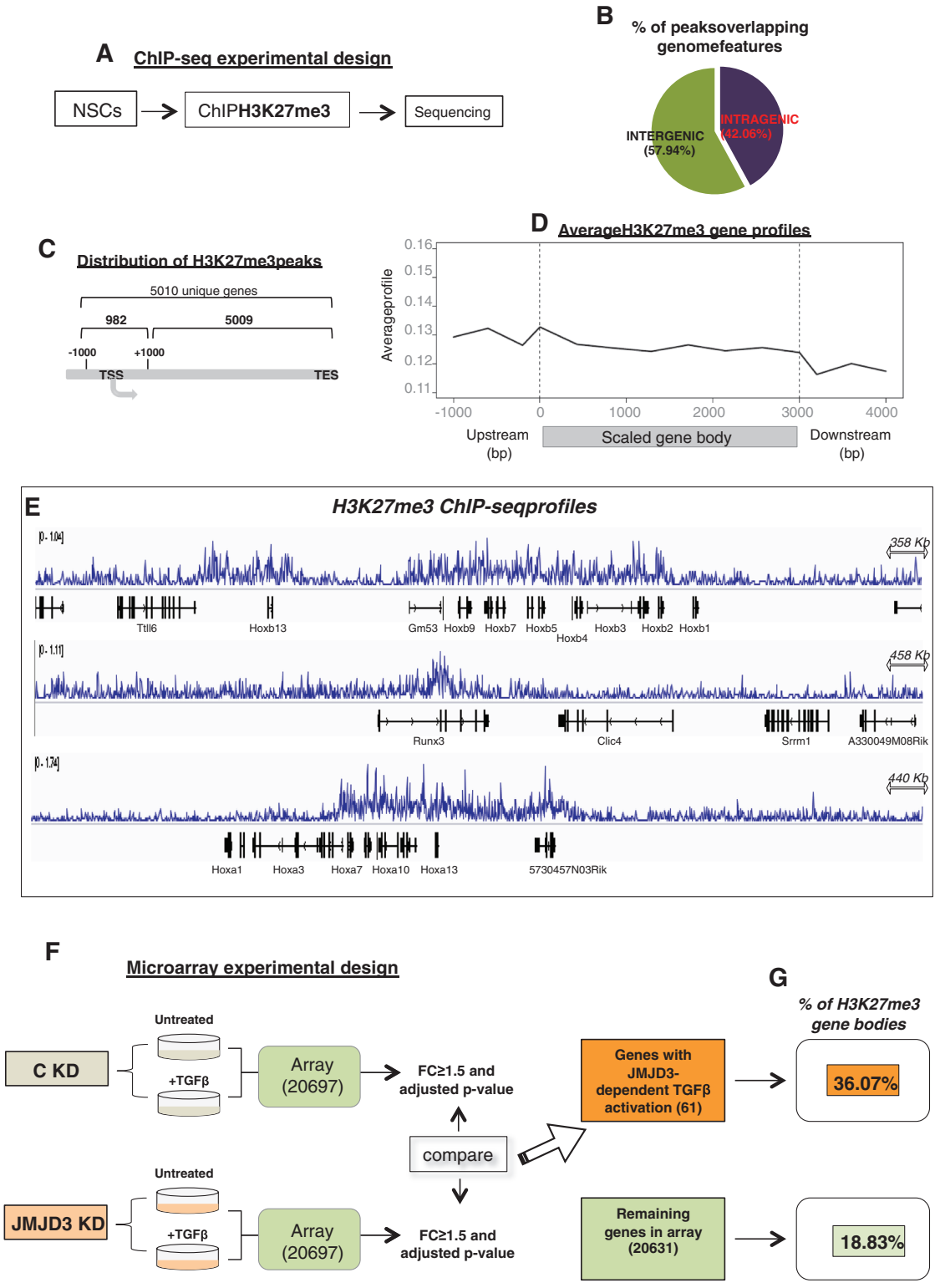

FIGURE 1: Genome-wide H3K27me3 distribution in NSCs. (A) The ChIP-seq experimental procedure. (B) Genomic distribution of H3K27me3-binding sites in NSCs. (C) Number of H3K27me3 peaks distributed along the TSS and gene bodies in NSCs. (D) Metagene profile of H3K27me3 in NSCs. To construct a metagene profile, gene bodies were scaled to 3 kb (see *Materials and Methods*). (E) Representation of H3K27me3 coverage by normalized wig files for the indicated RefSeq genes. Right numbers represent the length of the visualized region in kilobases. Left numbers indicate the scale of the *Y* axis (minimum and maximum numbers of reads). (F) Schematic representation of microarray analysis design to identify JDTA genes in NSCs. (G) Percentage of genes with H3K27me3 peaks on the gene body within the set of JDTA genes (orange box) and in the remaining genes in the array (green box).

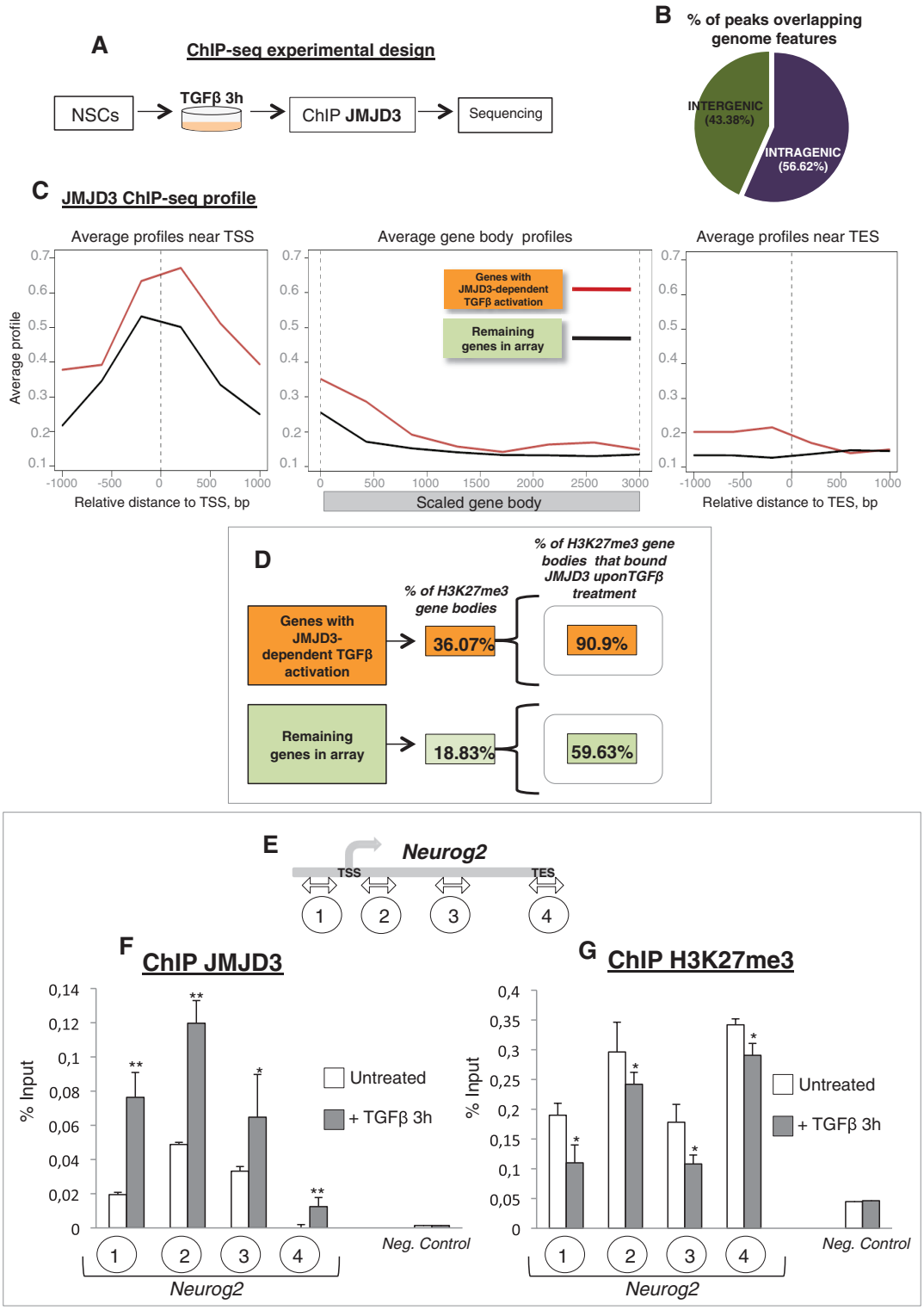

FIGURE 2: JMJD3 is recruited to the intragenic regions upon TGFβ signal. (A) The ChIP-seq experimental procedure. (B) Genomic distribution of JMJD3-binding sites in TGFβ-stimulated NSCs. (C) Metagene profiles of JMJD3 coverage for JDTA genes and for the remaining genes in the array (orange and green boxes, respectively) in TGFβ-stimulated NSCs. (D) Middle, schematic representation showing percentage of genes with H3K27me3 peaks within JDTA genes (orange box) or the remaining genes in the array (green box). Right, percentage of H3K27me3-enriched gene bodies bound by JMJD3 for JDTA genes (orange box) or for the remaining genes in the array (green box). (E) Schematic representation of the neurogenin 2 locus. The encircled numbers under the scheme indicate the location of the primer sets used in the ChIP experiments. (F, G) JMJD3 (F) and H3K27me3 (G) ChIP assays analyzed by qPCR performed in NSCs untreated (white bars) or TGFβ treated (3 h; gray bars). Regions analyzed for the neurogenin 2 locus and the negative control gene (G6pd2) are indicated in the *x*-axis. Mock (immunoglobulin G ChIP) signals were subtracted from specific enrichment values. Three biological replicates were used in each ChIP experiment. Error bars indicate SD. *$p < 0.05$; **$p < 0.01$.

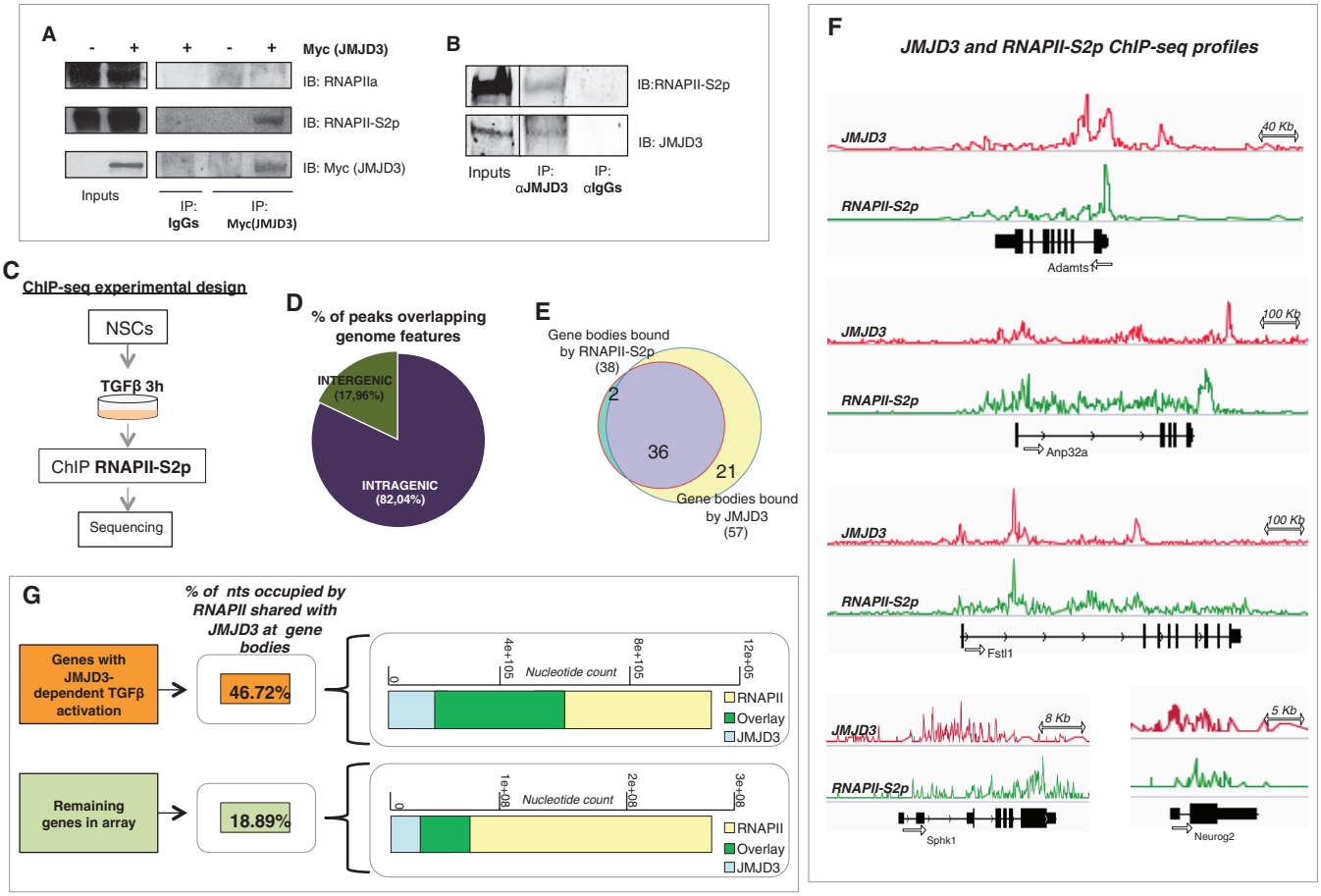

FIGURE 3: JMJD3 and RNAPII colocalize on TGFβ-regulated genes. (A, B) Immunoprecipitation of overexpressed Myc-JMJD3 (A) or endogenous JMJD3 (B) was performed using 293t (A) or NSC (B) total extracts. RNAPII or RNAPII-S2p were detected by immunoblotting. Input corresponds to 1% of the total protein present in the whole-cell extract. (C) The ChIP-seq experimental procedure. (D) Genomic distribution of RNAPII-S2p binding sites in TGFβ-stimulated NSCs. (E) Venn diagram showing the number of gene bodies cobound by JMJD3 and RNAPII-S2p from the set of JDTA genes. (F) Representation of RNAPII-S2p and JMJD3 coverage by normalized wig files for the indicated RefSeq genes. Right numbers represent the length of the visualized region. Left numbers indicate the scale of the *y*-axis (number of reads). (G) Overlapping nucleotides between RNAPII-S2p and JMJD3 from the set of JDTA genes (orange box) and the rest of the genes (green box).

coimmunoprecipitation (CoIP) experiments, we found that overexpressed JMJD3 interacts with the elongating form of RNAPII (phosphorylated at Ser-2; RNAPII-S2p) but not with unphosphorylated RNAPII (Figure 3A). We confirmed this result by CoIP experiments with endogenous proteins, which showed that JMJD3 and RNAPII-S2p interact in NSCs (Figure 3B), pointing to the possibility that JMJD3 forms part of the elongating complex.

JMJD3 and RNAPII colocalize along the gene bodies of TGFβ target genes

The ability of the JMJD3 and RNAPII-S2p to coimmunoprecipitate suggests that both factors could bind a subset of common target genes. To investigate this possibility, we identified the genomic binding sites of RNAPII-S2p in TGFβ-treated NSCs by sequencing DNA fragments of immunoprecipitated chromatin (Figure 3C). To perform the ChIP-seq experiment, we used a ChIP-grade antibody that efficiently immunoprecipitates the RNAPII-S2p form (Supplemental Figure S4A). We obtained 24,997 peaks for RNAPII-S2p after input normalization. Most of the peaks were associated with the intragenic regions, in agreement with RNAPII-S2p–elongating function (Figure 3D).

Because we were interested in JMJD3 association with RNAPII-S2p in JDTA genes, we investigated the occupancy of both factors on their gene bodies. We analyzed the number of genes that associate both JMJD3 and RNAPII-S2p factors. We observed JMJD3 bound to most of RNAPII-S2p–positive genes (Figure 3E). It is striking that high-resolution analysis showed that, on gene bodies, 46.72% of the nucleotides occupied by RNAPII-S2p were shared with JMJD3 (Figure 3G, orange box) in JDTA genes. This figure dropped to 18.89% for the remaining genes in the array (Figure 3G, green box). Similarly, 68.8% of RNAPII-S2p peaks (52 of 77) colocalize with JMJD3 peaks in the coding region of the JDTA genes (Supplemental Figure S4B). Figure 3F shows the colocalization of RNAPII-S2p and JMJD3 for five genes from the set of JDTA genes.

Taken together, these results indicate that, in TGFβ-stimulated NSCs, JMJD3 and RNAPII-S2p are broadly associated and distributed along the gene bodies of JDTA genes.

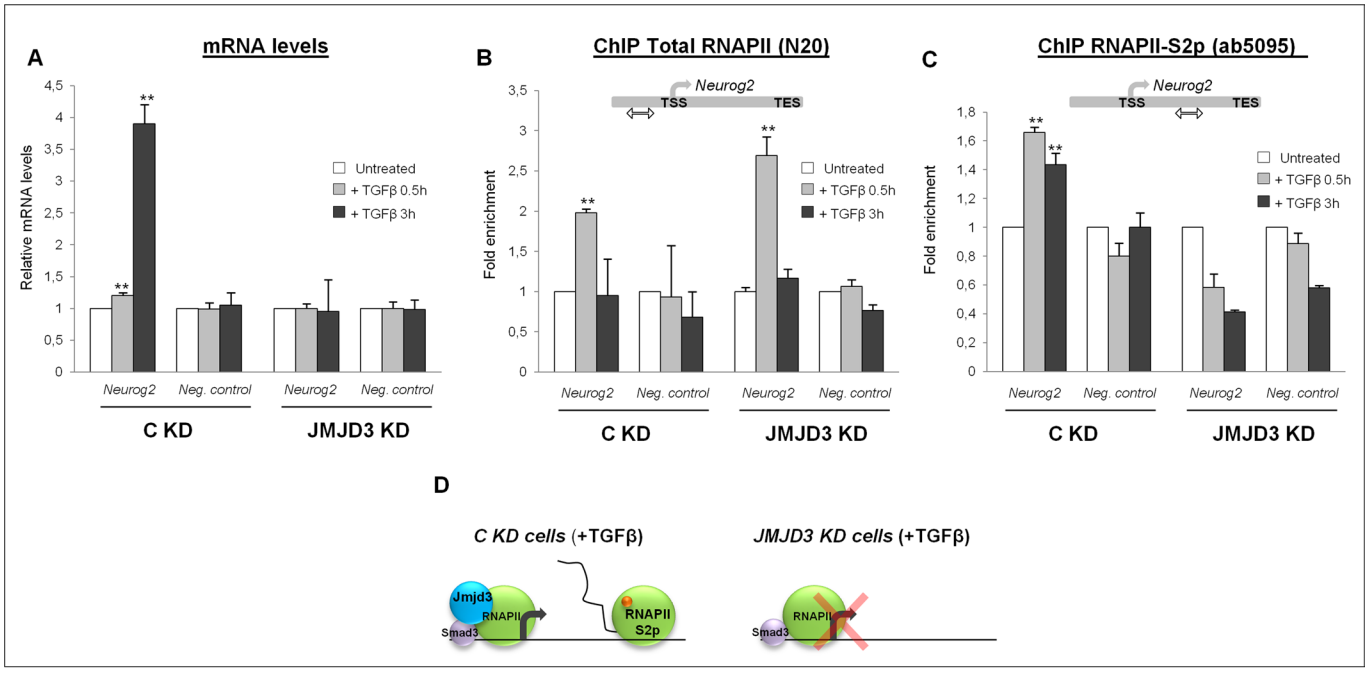

FIGURE 4: JMJD3 is essential for RNAPII elongation. (A) Relative mRNA levels of neurogenin 2 in C KD and JMJD3 KD NSCs untreated or treated with TGFβ for the times indicated in the legend. (B, C) ChIP assays analyzed by qPCR performed in C KD and JMJD3 KD NSC lines before (0 h) and after (0.5 and 3 h) TGFβ treatment using total RNAPII (N20; B) or RNAPII-S2p (ab5095; C) antibodies. Analyzed gene regions are indicated in the corresponding scheme. Normalized basal conditions and fold recruitment upon TGFβ treatment in C KD and JMJD3 KD cell lines are represented. (D) Summary of the results. In TGFβ-stimulated C KD cells the transcription machinery is uploaded to the promoters and spreads within the body of genes to generate new mRNA. In TGFβ-stimulated JMJD3 KD cells, the recruitment of RNAPII to promoters occurs to the same extent as in control cells, but the RNAPII progression along the gene bodies is impaired.

JMJD3 is essential for RNAPII elongation

To assess whether colocalization of JMJD3 with RNAPII-S2p plays any role in stimulating transcription, we analyzed the recruitment of RNAPII in the presence or absence of JMJD3, using C KD and JMJD3 KD NSCs. Then we performed ChIP assays on a JDTA gene (*Neurog2*) and a negative control gene (*G6pd2*) for both C KD and JMJD3 KD NSCs (Figure 4A and Estarás *et al.*, 2012) to investigate the RNAPII recruitment on *Neurog2* promoter upon TGFβ treatment, using an antibody that recognizes the N-terminus of RNAPII (N20). Results in Figure 4B indicate that RNAPII was targeted to the *Neurog2* promoter in the C KD cell line 0.5 h after TGFβ activation. Of interest, we observed similar behavior for RNAPII promoter association in the JMJD3 KD cell line (Figure 4B). These findings demonstrate that JMJD3 is not essential for RNAPII initial targeting to promoters.

Then we tested whether JMJD3 affects the levels of elongating RNAPII at transcribing regions upon TGFβ treatment. ChIP assays showed a clear enrichment in RNAPII-S2p on the *Neurog2* gene after TGFβ treatment in C KD cells, correlating with mRNA accumulation (Figure 4A). Of interest, this RNAPII-S2p recruitment was absent in JMJD3 KD cells (Figure 4C), in agreement with the lack of active transcription (Figure 4A). To further understand the influence of JMJD3 on RNAPII-S2p, we analyzed the recruitment of the P-TEFb elongation factor. The catalytic subunit of P-TEFb complex is Cdk9, which phosphorylates Ser-2 of the CTD domain of RNAPII. Apart from its extensive role as an essential factor for transcription elongation (Peterlin and Price, 2006), it was also found that Cdk9 phosphorylates Smad3, promoting its activity (Alarcon *et al.*, 2009). On that basis, we tested whether JMJD3 regulates Cdk9 binding to the promoters. To do that, we performed Cdk9 ChIP-qPCR experiments in C KD and JMJD3 KD cell lines in the absence and presence of TGFβ. The results (Supplemental Figure S5A) showed that Cdk9 is recruited to the *Neurog2* promoter in TGFβ-stimulated control cells. Nevertheless, the low levels of JMJD3 significantly affected Cdk9 binding to the *Neurog2* gene. These findings are in accordance with the lack of RNAPII-S2P observed in JMJD3 KD cells (Figure 4D). It is worth mentioning that the observed effect of JMJD3 on transcription is not because JMJD3 influences Smad3 binding to promoters (Estarás *et al.*, 2012) or affects Smad3 translocation into the nucleus upon TGFβ treatment (Supplemental Figure S5B). Overall these observations suggested that JMJD3 is required to allow RNAPII progression through the *Neurog2* gene body (Figure 4D).

JMJD3 binding to gene bodies depends on active transcription

The experiments described here showed that JMJD3 is distributed along the gene bodies of TGFβ-activated genes in association with RNAPII-S2p. We then sought to investigate whether the presence of JMJD3 in the intragenic regions require active transcription. To this end, we treated NSCs with DRB, a pharmacological inhibitor of transcriptional elongation. We first confirmed that under our experimental conditions (DRB, 75 μM, 4 h, added 1 h before TGFβ cytokine treatment), 1) DRB treatment blocked RNAPII Ser-2 phosphorylation (Figure 5A), and 2) TGFβ induced expression of the gene under study (Figure 5B). In addition, to rule out any nonspecific effect of the drug on TGFβ response, we confirmed that it did not affect Smad3 translocation into the nucleus after TGFβ stimulation (Figure 5C). We then examined JMJD3

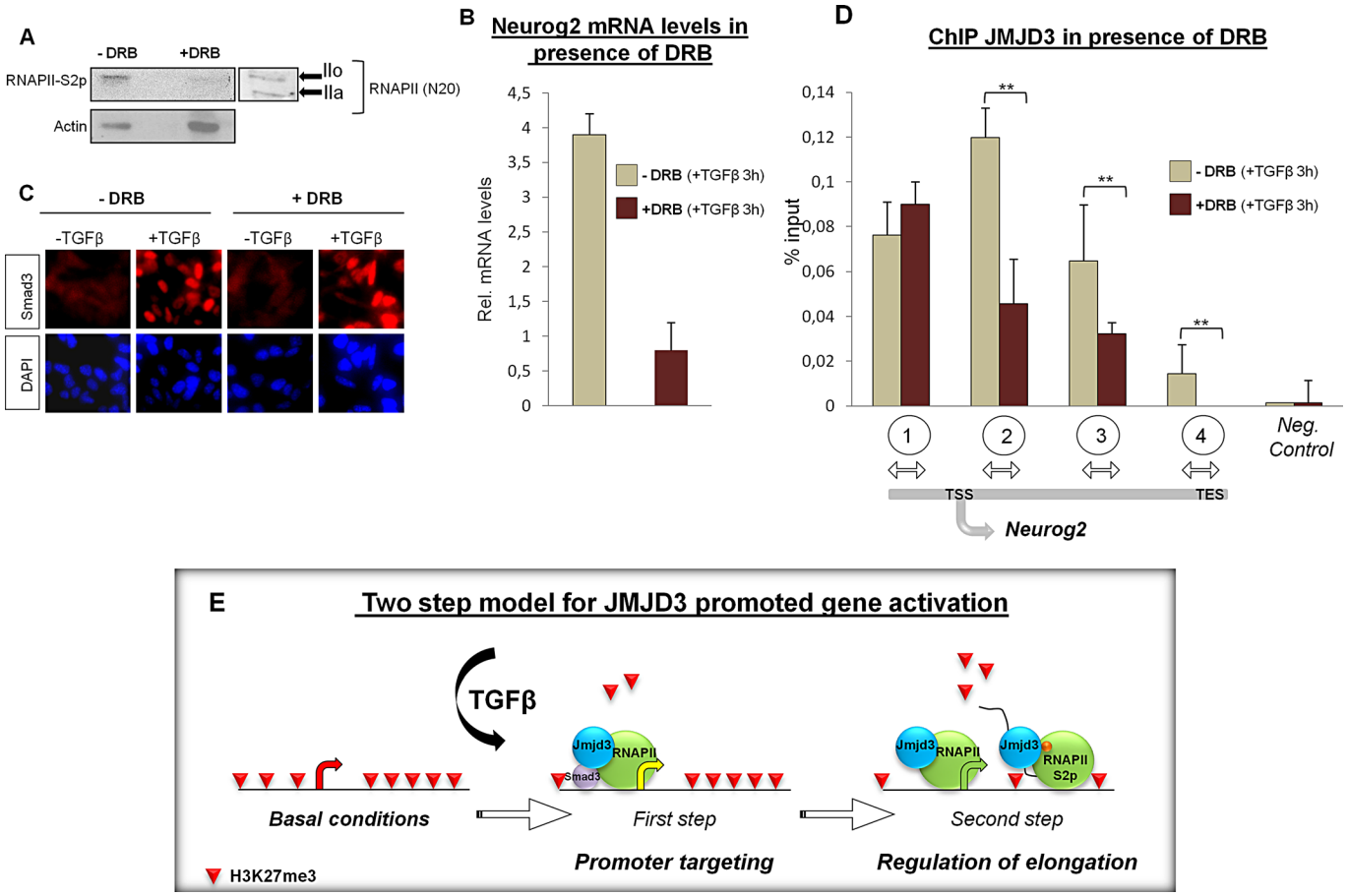

FIGURE 5: JMJD3 association within the body of genes depends on active transcription.(A) Immunoblot from NSCs using ab5095 antibody (which recognizes RNAPII-S2p isoform) in the absence (–DRB) or presence (+DRB) of 75 μM DRB for 4 h. Actin was used as loading control. Immunoblot using RNAPII antibody (N20; which recognizes both unphosphorylated [IIa] and phosphorylated [IIo] forms) was used to verify the specificity of ab5095 antibody band. (B) Neurogenin 2 mRNA levels in NSCs treated with TGFβ (3 h) in the absence (–DRB) or presence of DRB (+) analyzed by qPCR. (C) Immunostaining of NSCs with Smad3 antibody (red) before or after TGFβ treatment in the absence or presence of DRB. Images in blue are 4′,6-diamidino-2-phenylindole staining (DNA). (D) JMJD3 ChIP assays analyzed by qPCR in the absence (–DRB) or presence (+DRB) of DRB in TGFβ-stimulated NSCs (3 h). The encircled numbers above the scheme indicate the location of the primer sets used in the ChIP experiments. The negative control is the G6pd2 gene. Mock signals were subtracted from specific enrichment values. Three biological replicates were used in each ChIP experiment. Error bars indicate SD. $^{**}p < 0.01$. (E) Model for the TGFβ-dependent JMJD3 activation mechanism. The JMJD3 contribution to transcription regulation occurs through a two-step process. In the first step, JMJD3 is recruited to TGFβ-target genes by transcription factor Smad3 (Estarás *et al.*, 2012). In the second step, JMJD3 migrates into the H3K27me3-enriched gene bodies to regulate the process of transcriptional elongation.

recruitment within the transcribing regions upon TGFβ treatment. Analysis of JMJD3 ChIP in Figure 5D shows that TGFβ-induced JMJD3 enrichment within the gene body was impaired in the presence of DRB. Of interest, DRB treatment blocked specifically JMJD3 association to the intragenic regions, since JMJD3 binding to promoter was not affected (Figure 5D, region 1). These data demonstrate that the presence of JMJD3 in the gene bodies is linked to active transcription.

Overall these findings strongly support that JMJD3 HDM has a key role in gene bodies in allowing transcription elongation to proceed.

DISCUSSION

Our results provide new insights into the transcriptional regulatory mechanism mediated by JMJD3. In this study we show, using genome-wide experiments and further molecular analysis, that JMJD3 regulates the transcription of TGFβ-responsive genes by allowing RNAPII progression through the gene bodies. We demonstrate that the contribution of JMJD3 to transcription not only occurs at the promoter level (Estarás *et al.*, 2012), but also requires migration of JMJD3 to the H3K27me3 intragenic regions to regulate the process of transcriptional elongation (Figure 5E). The correlation between JMJD3 presence on gene bodies and H3K27me3 demethylation suggests that active demethylation at transcribing regions is important for RNAPII progression.

Our data show the existence of broad domains of H3K27me3 enrichment along the gene bodies. Similar data were previously reported (Hawkins *et al.*, 2010; Young *et al.*, 2011), showing that H3K27me3 domains are expanded on committed cells. Our study not only confirms the H3K27me3 expansion along the transcribing regions, but it also sheds light on the mechanism by which intragenic H3K27me3 demethylation is coupled to transcriptional elongation.

Our results show that with TGFβ, JMJD3 and RNAPII-S2p spread along the H3K27me3 intragenic regions to transcribe the genes and that in the absence of JMJD3, RNAPII-S2p is not able to progress through the H3K27me3-enriched genes. This suggests that H3K27me3 demethylation at the intragenic regions might provide an additional requirement to trigger transcriptional activation. It is also possible that other factors different from histones might be JMJD3 targets, such as Smads, RNAPII, or other components of the transcription machinery. However, the fact that JMJD3 is required to activate only a subset of genes in response to TGFβ suggests that the major JMJD3 target is not a general transcription factor. Another possibility is that JMJD3 (in addition to its HDM function) plays a demethylating-independent role for these genes, as proposed for other genes (Miller *et al.*, 2010).

There are several examples of factors that spread along the transcribing region of genes with RNAPII, such as the RNA processing machinery (Pandit *et al.*, 2008). This is also the case for UTX, which is associated with the intragenic region of genes transcribed by RNAPII (Seenundun *et al.*, 2010) and colocalizes with the elongating form of RNAPII (Smith *et al.*, 2008). Moreover, it was recently shown that JMJD3 and UTX activate T-box family–dependent gene transcription by interacting with Brg1 (Miller *et al.*, 2010). Of interest, Brg1 facilitates transcription elongation (Subtil-Rodriguez and Reyes, 2010). Thus JMJD3 may promote RNAPII progression through the gene bodies by altering their chromatin architecture, by H3K27me3 demethylation of the transcribing regions, and possibly through the interaction with Brg1 or other chromatin-modifying factors. It was also recently shown that JMJD3, together with KIAA1718 histone demethylase, promotes transcription elongation by contributing to the recruitment of SPT6 and SPT16 elongation factors to gene promoters in response to TPA (Chen *et al.*, 2012). Accordingly, we show that JMJD3 contributes to the recruitment of the Ser2P-CTD kinase Cdk9 on the neurogenin 2 promoter. Taken together, these results point to multiple roles of JMJD3 in transcription elongation probably through HDM activity–dependent and –independent mechanisms.

Whether the proposed JMJD3 role is specific for the TGFβ signaling pathway needs further investigation. However, given the wide spectrum of signaling pathways that act through JMJD3 activity (Jepsen *et al.*, 2007; De Santa *et al.*, 2009; Akizu *et al.*, 2010; Estarás *et al.*, 2012), we postulate that it may be a general mechanism to activate genes silenced by H3K27me3. Nonetheless, due to the regulatory function of TGFβ in developmental processes and in cancer, our discovery provides an additional layer for the modulation of TGFβ signaling pathway outcome, targeting JMJD3 activity on a specific set of TGFβ-responsive genes.

MATERIALS AND METHODS

Cell culture

Human 293t cells were grown under standard conditions (Blanco-Garcia *et al.*, 2009). Mouse NSCs were grown as previously described (Estarás *et al.*, 2012).

Antibodies and reagents

TGFβ was acquired from Millipore (Billerica, MA; GF111), and DRB was purchased from Sigma-Aldrich (St. Louis, MO). Antibodies used were anti–rabbit trimethyl H3K27 (07449; Millipore), rabbit total RNAPII (N20; sc-899x; Santa Cruz Biotechnology, Santa Cruz, CA), rabbit RNAPII-S2p ChIP grade (ab5095; Abcam, Cambridge, MA), mouse RNAPII 8WG16 (ab817; Abcam), rabbit Cdk9 (H-169; sc-8338; Santa Cruz Biotechnology), goat actin (I-19; sc-1616; Santa Cruz Biotechnology), mouse β-tubulin (MAB3408; Millipore), rabbit histone H3 (ab1791; Abcam), and rabbit Smad3 (ab28379; Abcam). Anti-rabbit JMJD3 was kindly provided by K. Helin (Agger *et al.*, 2009).

Cytoplasmic and nuclear fractionation

Cell fractionation was carried out starting from 3×10^6 NSCs untreated or treated with TGFβ (5 ηg/ml) for 3 h. Cell pellets were resuspended in buffer A (10 mM Tris, 10 mM KCl, 1.5 mM $MgCl_2$, and protease inhibitors) and kept on ice for 10 min. After centrifugation at $1500 \times g$ for 5 min, pellets were resuspended in buffer B (buffer A and 1% NP40) and incubated on ice for 5 min before centrifugation at $5000 \times g$ for 5 min. Supernatant contained the cytosolic fraction. Pellet was resuspended in buffer C (20 mM Tris, 420 mM NaCl, 1.5 mM $MgCl_2$, 25% glycerol, 0.2 mM EDTA, and protease inhibitors) by vortexing and incubating on ice. Lysates were then centrifuged at the highest speed for 20 min at 4°C, and supernatant was collected (nuclear fraction). Extracts were then used for Immunoblotting.

Coimmunoprecipitation and ChIP assays

Coimmunoprecipitation experiments were performed as previously described (Estarás *et al.*, 2012).

Chromatin immunoprecipitation assays were essentially performed as described (Frank *et al.*, 2001; Valls *et al.*, 2007) with modifications: 3×10^6 NSCs untreated or treated with TGFβ (5 ng/ml, for the indicated times) were fixed with 0.2 mM di-(*N*-succinimidyl) glutarate (Sigma-Aldrich), 45 min at room temperature, followed by formaldehyde 1%, 20 min. Fixation was stopped by addition of 0.125 mM glycine. The sonication step was performed in a Bioruptor sonicator (12 min, 30 s on, 30 s off), and 1 mg of protein was used for each immunoprecipitation. Antibody–protein complex was captured with preblocked protein A (Amersham-Pharmacia Biotech, GE Healthcare Bio-Sciences, Piscataway, NJ), and DNA purification was carried out using Nucleospin Extract II (Macherey-Nagel, Bethlehem, PA) columns. ChIP DNA was analyzed by qPCR with SYBR Green (Roche, Indianapolis, IN) in a LightCycler 480 PCR system (Roche) using the primers specified in Supplemental Table S2.

ChIP-seq procedure

Chromatin immunoprecipitation and preparation of samples for sequencing were done essentially as previously described (Estarás *et al.*, 2012). Before sequencing, ChIP DNA was prepared by simultaneously blunting, repairing, and phosphorylating ends according to manufacturer's instructions (Illumina, San Diego, CA). The DNA was adenylated at the 3′ end and recovered by QIAquick PCR purification kit (Qiagen, Valencia, CA) according to the manufacturer's recommendations. Adaptors were added by ligation, and the ligated fragments were amplified by PCR, resolved in a gel, and purified by Qiagen columns. Samples were loaded into individual lanes of the flow cell. We generated >26 million 36–base pair reads for each ChIP sample. Reads were mapped with bowtie (Langmead *et al.*, 2009) to the University of California, Santa Cruz (Fujita *et al.*, 2011), *Mus musculus* genome, release 9; only sequence reads mapping at unique locations were kept. Peaks were called with SICER (Zang *et al.*, 2009) on each sample with Input as control. PeakAnalyzer (Salmon-Divon *et al.*, 2010) and CEAS (Ji *et al.*, 2006) were used for peak annotation and profiling. R language and Bioconductor (Gentleman *et al.*, 2004), including packages ShortRead and IRanges (Morgan *et al.*, 2009), were used for further annotation and statistical analysis.

To derive the metagene profile, we first computed the profile for each gene before computing the average. Specifically, we divided

each gene into the same number of bins and computed the genomic sequencing read densities for each bin. Genes are scaled as follows: 1) ±1 kb from the TSS and ±1 kb from the TES were unscaled, and 2) the region within the gene body extending from TSS to TES was scaled to 3 kb.

mRNA extraction and qPCR

mRNA was purified with Qiagen columns following the manufacturer's instructions. Reverse transcription was performed with Transcriptor kit (Roche) following the manufacturer's procedure. qPCR was done with SYBR Green in an LC480 LightCycler using the primers specified in Supplemental Table S2.

Indirect immunofluorescence

Indirect immunofluorescence was essentially performed as described previously (Akizu *et al*., 2010).

Statistical analysis

Quantitative data are expressed as mean and SD of at least three biologically independent experiments. The significance of differences between groups was assessed using the Student's *t* test (*$p < 0.05$; **$p < 0.01$).

Accession numbers

The genome-wide mapping data of H3K27me3, JMJD3, and RNAPII in NSCs reported in the article are available at the Gene Expression Omnibus server (www.ncbi.nlm.nih.gov/geo/) with the accession number GSE38269.

ACKNOWLEDGMENTS

We thank K. Helin and J. C. Reyes for reagents and X. de la Cruz and A. García for suggestions. This study was supported by Grants BFU2006-01493, CSD2006-00049, and BFU2009-11527 to M.A.M.B. from the Spanish Ministry of Education and Science and 090210 from the Fundaciò La Marató de TV3 to M.M.B. C.E. and N.A. were recipients of FPU and I3P (I3P-BPD2005) fellowships, respectively.

REFERENCES

Agger K, Cloos PA, Christensen J, Pasini D, Rose S, Rappsilber J, Issaeva I, Canaani E, Salcini AE, Helin K (2007). UTX and JMJD3 are histone H3K27 demethylases involved in HOX gene regulation and development. Nature 449, 731–734.

Agger K, Cloos PA, Rudkjaer L, Williams K, Andersen G, Christensen J, Helin K (2009). The H3K27me3 demethylase JMJD3 contributes to the activation of the INK4A-ARF locus in response to oncogene- and stress-induced senescence. Genes Dev 23, 1171–1176.

Akizu N, Estaras C, Guerrero L, Marti E, Martinez-Balbas MA (2010). H3K27me3 regulates BMP activity in developing spinal cord. Development 137, 2915–2925.

Alarcon C *et al*. (2009). Nuclear CDKs drive Smad transcriptional activation and turnover in BMP and TGF-beta pathways. Cell 139, 757–769.

Barski A, Cuddapah S, Cui K, Roh TY, Schones DE, Wang Z, Wei G, Chepelev I, Zhao K (2007). High-resolution profiling of histone methylations in the human genome. Cell 129, 823–837.

Blanco-Garcia N, Asensio-Juan E, de la Cruz X, Martinez-Balbas MA (2009). Autoacetylation regulates P/CAF nuclear localization. J Biol Chem 284, 1343–1352.

Boyer LA *et al*. (2006). Polycomb complexes repress developmental regulators in murine embryonic stem cells. Nature 441, 349–353.

Bracken AP, Dietrich N, Pasini D, Hansen KH, Helin K (2006). Genome-wide mapping of Polycomb target genes unravels their roles in cell fate transitions. Genes Dev 20, 1123–1136.

Burgold T, Spreafico F, De Santa F, Totaro MG, Prosperini E, Natoli G, Testa G (2008). The histone H3 lysine 27-specific demethylase Jmjd3 is required for neural commitment. PLoS One 3, e3034.

Cao R, Wang L, Wang H, Xia L, Erdjument-Bromage H, Tempst P, Jones RS, Zhang Y (2002). Role of histone H3 lysine 27 methylation in Polycomb-group silencing. Science 298, 1039–1043.

Chen S *et al*. (2012). The histone H3 Lys 27 demethylase JMJD3 regulates gene expression by impacting transcriptional elongation. Genes Dev 26, 1364–1375.

Czermin B, Melfi R, McCabe D, Seitz V, Imhof A, Pirrotta V (2002). *Drosophila* enhancer of Zeste/ESC complexes have a histone H3 methyltransferase activity that marks chromosomal Polycomb sites. Cell 111, 185–196.

De Santa F *et al*. (2009). Jmjd3 contributes to the control of gene expression in LPS-activated macrophages. EMBO J 28, 3341–3352.

De Santa F, Totaro MG, Prosperini E, Notarbartolo S, Testa G, Natoli G (2007). The histone H3 lysine-27 demethylase Jmjd3 links inflammation to inhibition of polycomb-mediated gene silencing. Cell 130, 1083–1094.

Estarás C, Akizu N, García A, Beltrán S, de la Cruz X, Martínez-Balbás M (2012). Genome-wide analysis reveals that Smad3 and JMJD3 HDM co-activate the neural developmental program. Development 139, 2681–2691.

Frank SR, Schroeder M, Fernandez P, Taubert S, Amati B (2001). Binding of c-Myc to chromatin mediates mitogen-induced acetylation of histone H4 and gene activation. Genes Dev 15, 2069–2082.

Fujita PA *et al*. (2011). The UCSC Genome Browser database: update 2011. Nucleic Acids Res 39, D876–D882.

Gentleman RC *et al*. (2004). Bioconductor: open software development for computational biology and bioinformatics. Genome Biol 5, R80.

Hawkins RD *et al*. (2010). Distinct epigenomic landscapes of pluripotent and lineage-committed human cells. Cell Stem Cell 6, 479–491.

Jepsen K, Solum D, Zhou T, McEvilly RJ, Kim HJ, Glass CK, Hermanson O, Rosenfeld MG (2007). SMRT-mediated repression of an H3K27 demethylase in progression from neural stem cell to neuron. Nature 450, 415–419.

Ji X, Li W, Song J, Wei L, Liu XS (2006). CEAS: *cis*-regulatory element annotation system. Nucleic Acids Res 34, W551–W554.

Kim SW, Yoon SJ, Chuong E, Oyolu C, Wills AE, Gupta R, Baker J (2011). Chromatin and transcriptional signatures for Nodal signaling during endoderm formation in hESCs. Dev Biol 357, 492–504.

Kuzmichev A, Nishioka K, Erdjument-Bromage H, Tempst P, Reinberg D (2002). Histone methyltransferase activity associated with a human multiprotein complex containing the Enhancer of Zeste protein. Genes Dev 16, 2893–2905.

Lan F *et al*. (2007). A histone H3 lysine 27 demethylase regulates animal posterior development. Nature 449, 689–694.

Langmead B, Trapnell C, Pop M, Salzberg SL (2009). Ultrafast and memory-efficient alignment of short DNA sequences to the human genome. Genome Biol 10, R25.

Lee MG, Villa R, Trojer P, Norman J, Yan KP, Reinberg D, Di Croce L, Shiekhattar R (2007). Demethylation of H3K27 regulates polycomb recruitment and H2A ubiquitination. Science 318, 447–450.

Lee MG, Wynder C, Bochar DA, Hakimi MA, Cooch N, Shiekhattar R (2006). Functional interplay between histone demethylase and deacetylase enzymes. Mol Cell Biol 26, 6395–6402.

Lois S, Akizu N, de Xaxars GM, Vazquez I, Martinez-Balbas M, de la Cruz X (2010). Characterization of structural variability sheds light on the specificity determinants of the interaction between effector domains and histone tails. Epigenetics 5, 137–148.

Margueron R, Reinberg D (2011). The Polycomb complex PRC2 and its mark in life. Nature 469, 343–349.

Mikkelsen TS *et al*. (2007). Genome-wide maps of chromatin state in pluripotent and lineage-committed cells. Nature 448, 553–560.

Miller SA, Mohn SE, Weinmann AS (2010). Jmjd3 and UTX play a demethylase-independent role in chromatin remodeling to regulate T-box family member-dependent gene expression. Mol Cell 40, 594–605.

Morey L, Helin K (2010). Polycomb group protein-mediated repression of transcription. Trends Biochem Sci 35, 323–332.

Morgan M, Anders S, Lawrence M, Aboyoun P, Pages H, Gentleman R (2009). ShortRead: a bioconductor package for input, quality assessment and exploration of high-throughput sequence data. Bioinformatics 25, 2607–2608.

Pan G, Tian S, Nie J, Yang C, Ruotti V, Wei H, Jonsdottir GA, Stewart R, Thomson JA (2007). Whole-genome analysis of histone H3 lysine 4 and lysine 27 methylation in human embryonic stem cells. Cell Stem Cell 1, 299–312.

Pandit S, Wang D, Fu XD (2008). Functional integration of transcriptional and RNA processing machineries. Curr Opin Cell Biol 20, 260–265.

Peterlin BM, Price DH (2006). Controlling the elongation phase of transcription with P-TEFb. Mol Cell 23, 297–305.

Salmon-Divon M, Dvinge H, Tammoja K, Bertone P (2010). PeakAnalyzer: genome-wide annotation of chromatin binding and modification loci. BMC Bioinformatics 11, 415.

Seenundun S, Rampalli S, Liu QC, Aziz A, Palii C, Hong S, Blais A, Brand M, Ge K, Dilworth FJ (2010). UTX mediates demethylation of H3K27me3 at muscle-specific genes during myogenesis. EMBO J 29, 1401–1411.

Sen GL, Webster DE, Barragan DI, Chang HY, Khavari PA (2008). Control of differentiation in a self-renewing mammalian tissue by the histone demethylase JMJD3. Genes Dev 22, 1865–1870.

Smith ER, Lee MG, Winter B, Droz NM, Eissenberg JC, Shiekhattar R, Shilatifard A (2008). *Drosophila* UTX is a histone H3 Lys27 demethylase that colocalizes with the elongating form of RNA polymerase II. Mol Cell Biol 28, 1041–1046.

Subtil-Rodriguez A, Reyes JC (2010). BRG1 helps RNA polymerase II to overcome a nucleosomal barrier during elongation, in vivo. EMBO Rep 11, 751–757.

Valls E, Blanco-Garcia N, Aquizu N, Piedra D, Estaras C, de la Cruz X, Martinez-Balbas MA (2007). Involvement of chromatin and histone deacetylation in SV40 T antigen transcription regulation. Nucleic Acids Res 35, 1958–1968.

Young MD, Willson TA, Wakefield MJ, Trounson E, Hilton DJ, Blewitt ME, Oshlack A, Majewski IJ (2011). ChIP-seq analysis reveals distinct H3K27me3 profiles that correlate with transcriptional activity. Nucleic Acids Res 39, 7415–7427.

Zang C, Schones DE, Zeng C, Cui K, Zhao K, Peng W (2009). A clustering approach for identification of enriched domains from histone modification ChIP-Seq data. Bioinformatics 25, 1952–1958.